PROGRESS TOWARDS A GLOBAL DIGITAL ELEVATION MODEL FOR MERCURY. Kris J. Becker[1] (kbecker@usgs.gov), Tammy L. Becker[1], Kenneth L. Edmundson[1], Robert W. Gaskell[2], Ralph L. McNutt, Jr.[3], Scott L. Murchie[3], Gregory A. Neumann[4], Mark E. Perry[3], Louise M. Prockter[3], Mark S. Robinson[5], Sean C. Solomon[6,7], Grant K. Stephens[3], F. Scott Turner[3], and Lynn A. Weller[1], [1]Astrogeology Science Center, United States Geological Survey, Flagstaff, AZ 86001; [2]Planetary Science Institute, 1700 East Fort Lowell, Suite 106, Tucson, AZ 85719; [3]Johns Hopkins University Applied Physics Laboratory, Laurel, MD 20723; [4]NASA Goddard Space Flight Center, Greenbelt, MD 20771; [5]School of Earth and Space Exploration, Arizona State University Tempe, AZ, 85287; [6]Lamont-Doherty Earth Observatory, Columbia University, Palisades, NY 10964; [7]Department of Terrestrial Magnetism, Carnegie Institution of Washington, Washington, DC 20015.

Introduction: A key objective of the MErcury Surface, Space ENvironment, GEochemistry, and Ranging (MESSENGER) mission [1] is to collect and characterize global topographic measurements with the Mercury Dual Imaging System (MDIS) narrow-angle camera (NAC) and multispectral wide-angle camera (WAC) [2], the Mercury Laser Altimeter (MLA) [3], and radio frequency occultation (RFO) timing [4].

MDIS stereo observations allow estimates of global topography at a relatively uniform scale (64 pixels/degree). In contrast, MLA collects high-resolution (350 to 450 m) topographic profiles only in the northern hemisphere, because of MESSENGER's highly eccentric orbit and high northern periapsis. RFO measurements are also collected as MESSENGER passes behind Mercury relative to the Earth, providing single-point estimates of radius. From these data, a global digital elevation model (DEM) will be created to support geophysical and geological investigations and provide the basis for future mission planning (e.g., BepiColombo [5]).

Methodology: A topographic model of the northern hemisphere of Mercury [6] was constructed from MLA measurements acquired through the second year of orbital operations (>14 million returns). MLA collects measurements at distances up to 1500 km with a range accuracy better than 20 m [6]. The horizontal resolution of MLA measurements depends on latitude, as determined by MESSENGER's altitude.

RFO measurements determine long-wavelength characteristics of Mercury's shape [4] and are particularly useful in the southern hemisphere, where no MLA observations are possible. Southern hemisphere RFO data, combined with MLA northern hemisphere measurements, provide a baseline product for direct comparison with DEMs derived from MDIS stereophotogrammetry and stereophotoclinometry (SPC).

MDIS images provide the means to create regional [7] and global [8] DEMs using several different techniques, including sparse sample control-point networks (CPNs), continuous sample stereo, continuous sample stereophotoclinometry, and limb profiles [9].

SPC procedures rely on variations in illumination in areas of image overlap, as well as parallax and limb data, and were applied to MDIS NAC and WAC images to create a global DEM [10]. The solution also returns updated MDIS focal lengths from clear-filter star observations.

WAC G filter images and NAC images were used to derive a global control-point network of common feature interest points [8]. The WAC G filter was selected because its passband overlaps that of the NAC, making automated image matching techniques more reliable. Each control point is associated with a well-defined surface feature contained within the field of view of at least two or more images. A least-squares bundle adjustment [11] was performed, providing improved image pointing parameters and triangulated control point coordinates. For each control point, a radius value was then computed, resulting in a discontinuous global point cloud from which a DEM was derived by interpolation techniques.

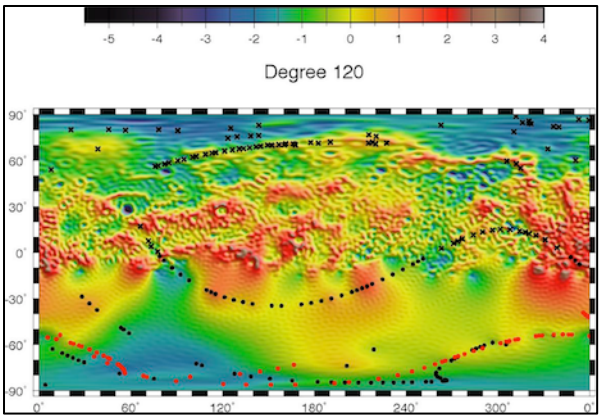

Figure 1. Shape model created from MLA and RFO. The black and red dots represent archived RFO points taken at different times. The map shows color-coded heights above the 2440 reference radius in km for a spherical harmonic solution expanded to degree and order 120 (~64 km block size).

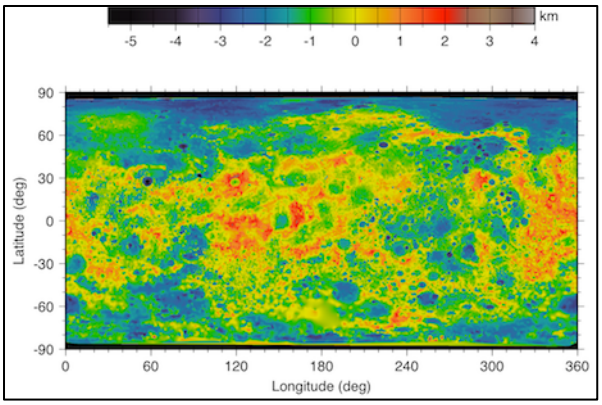

Figure 2. CPN DEM produced with an updated MDIS thermal model. The color scheme and mapping is the same as that in **Fig. 1**.

Discussion: The MLA/RFO northern hemisphere DEM is stored in a global equirectangular projection, sampled at 64 pixels/degree (665 m/pixel). MLA coverage is better than 80% north of the equator at ~4

pixels/degree, with spot sizes ranging between 15 and 100 m in diameter, ~400 m apart [6]. To extend these data to a global DEM, 239 non-uniformly distributed RFO points were introduced and a spherical harmonic expansion was derived via least squares (**Fig. 1**).

In early comparisons of the northern hemisphere (50°N to 85°N) between the CPN and MLA/RFO DEMs, a ~300 m high elevation bias was observed and found to be largely due to temperature-dependent changes in focal lengths of the WAC and NAC cameras. Temperature-dependent focal length (FL) models for the WAC clear filter and NAC were derived from star calibration measurements taken as the optics temperature varied. This initial model reduced about half of the discrepancy between the CPN point cloud and MLA to 147 m. Additional improvements were made to the WAC clear temperature-dependent FL model from the MDIS SPC DEM solution. A simple linear scaling of the first term of the fifth-order polynomial of the WAC clear-filter FL model provides thermal corrections for the remaining 11 WAC filters.

With the latest temperature-dependent FL model, a new CPN bundle adjustments was computed, and the average offset with MLA/RFO was reduced to 18 m. The CPN contains 263,762 CPN radius points from 21,498 images (**Fig. 2**) from which a 64 pixel/degree continuous DEM was interpolated. The region of comparison with the MLA/RFO is predominantly covered with WAC images, so no meaningful conclusion can be made about the accuracy of the NAC FL model at this time. The adjustment software, including the new MDIS camera model, are available in the Integrated System for Imagers and Spectrometers (ISIS3 3.4.5 public release) [8].

Long-wavelength Analysis: The three DEMs (MLA/RFO, SPC, CPN) are compared in **Fig. 3**. In the 35°N to 85°N latitude range there is relatively good agreement among all three datasets, consistent with improvements seen in the WAC temperature model. Southward of 35°N to the equator, inconsistencies are observed in the median data between the SPC and CPN as well as a larger range of elevation differences (black dots) between the CPN and MLA/RFO. This region has an increasing number of NAC images in the CPN. The SPC procedure uses all available MDIS images (WAC and NAC) and is less affected by NAC images in this region than the CPN.

A sharp transition south of 10°S corresponds to an abrupt change from WAC images to NAC images in the CPN solution. The disparity between CPN and SPC widens markedly to ~30°S, most likely due to an increase in number of NAC images in the CPN data, whereas more WAC images are included in this region in the SPC data. In the region between 50°S and 70°S, there is a reduction in WAC coverage, and NAC images dominate in the CPN, likely contributing to the offset relative to the SPC.

There is nearly a 1 km difference in elevation near the south pole between the MLA/RFO DEM and both the SPC and CPN datasets. However, this region is entirely populated with sparse RFO measurements and interpolated data in the MLA/RFO DEM. MDIS observations at the south pole are predominantly with NAC and have the largest pixel scales due to MESSENGER's eccentric orbit. In addition, some portions of Mercury's poles are in permanent shadow, resulting in a lack of illuminated MDIS data at the highest latitudes. It is likely that remaining residuals in the NAC FL thermal correction and large swaths of permanent shadow result in the gradual increase in elevation very near the south pole in both the CPN and SPC (**Fig. 3**). Improvements to the NAC temperature-dependent model may help reduce this south polar mismatch.

Conclusion: Parallel topographic data reduction efforts are underway to better understand the intricacies of each approach and to provide the best possible calibrations to allow for eventual production of a high-quality global DEM for Mercury. The MDIS WAC (and likely also the NAC) exhibits focal length fluctuations that correlate with temperature. A temperature-dependent component was added to the camera models for the MDIS WAC and NAC that improves DEM precision. Products derived from the CPN work also include controlled monochrome and color base maps.

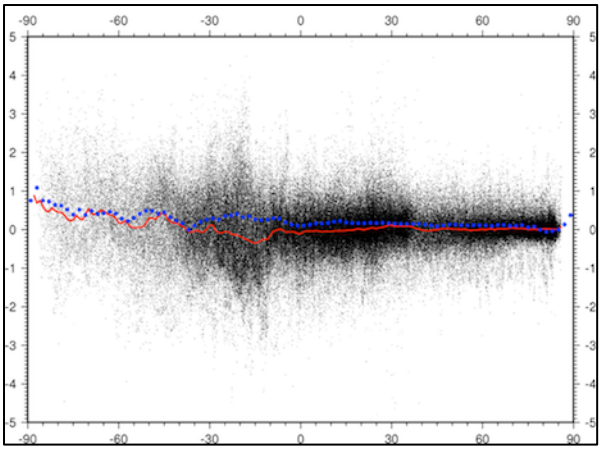

Figure 3. Difference in elevation (km) between the CPN point cloud and MLA/RFO DEMs (black dots), plotted versus latitude (degrees). Also shown are the median difference in a 2°-wide latitude filter (red) of the CPN and the MLA/RFO and the median difference between the SPC model and the MLA/RFO DEM (blue).

Future Work: We are pursuing refinements in the NAC temperature-dependent model that will likely improve the southern hemisphere control network and thus DEM precision. Work is also in progress to create a WAC-only DEM that should be helpful in assessing southern hemisphere dataset characteristics. A global DEM product is planned for release to the Planetary Data System.

References: [1] Solomon S. C. et al. (2001) *Planet. Space Sci.*, *49*, 1445-1465. [2] Hawkins S. E. III. et al. (2007) *Space Sci. Rev., 131,* 247-338. [3] Cavanaugh J. F. et al. (2007) *Space Sci. Rev., 131,* 451-480. [4] Perry M. E. et al. (2013) *LPS, 44*, abstract 2485. [5] Benkhoff J. et al. (2010) *Planet. Space Sci., 58*, 2-20. [6] Zuber M. T. et al. (2012) *Science*, *336*, 217-220. [7] Pruesker F. et al. (2011) *Planet. Space Sci.*, *59*, 1910-1917. [8] Becker K. J. et al. (2013) *LPS, 44*, abstract 2829. [9] Elgner S. et al. (2012) *LPS, 43*, abs. 1469. [10] Gaskell R.W. et al. (2008) *Meteorit. Planet. Sci.*, *43*, 1049-1061. [11] Edmundson K. L. et al. (2011) *GSA Abstracts with Program, 43*, paper 100-6, p. 267.